AN ABSTRACT OF A DISSERTATION

P-VERSION REFINEMENT STUDIES IN THE BOUNDARY
ELEMENT METHOD

Sivakkumar Arjunon

Doctor of Philosophy in Engineering

Two weakly singular forms of the hypersingular boundary integral
equation (HBIE) in three-dimensional potential theory are presented. The
hypersingular and singular integrals in the HBIE were regularized, either
over the entire boundary of the domain using a linear state representa-
tion of the density function, or locally in the vicinity of the source point,
expressing the added back terms as a combination of weakly singular geo-
metric curvature integrals , path integrals transformed by Stokes' theorm
and differential solid angle integrals. A new computational strategy which
follows an external limit to the boundary of the domain is introduced for
the locally regularized boundary element method (BEM). With this ap-
proach, the free term is computed as part of the regularization and no
special treatment is required for corners and edges. The regularized inte-
grals and the added back terms are computed using numerical integration
schemes.

The weakly singular boundary integral forms were implemented for
two geometries, a tetrahedron obviously dominated by edges and corners
and a sphere chosen to demonstrate generality for arbitrary curved sur-
faces. The results show significant improvements in accuracy with every
p-version refinement. For a given element order the locally regularized
form is shown to be more accurate than the globally regularized form.

P-VERSION REFINEMENT STUDIES IN THE BOUNDARY ELEMENT METHOD

A Dissertation

Presented to

the Faculty of the Graduate School

Tennessee Technological University

by

Sivakkumar Arjunon

In Partial Fulfillment

of the Requirements for the Degree

DOCTOR OF PHILOSOPHY

Engineering

May 2009

UMI Number: 3356389

INFORMATION TO USERS

The quality of this reproduction is dependent upon the quality of the copy submitted. Broken or indistinct print, colored or poor quality illustrations and photographs, print bleed-through, substandard margins, and improper alignment can adversely affect reproduction.

In the unlikely event that the author did not send a complete manuscript and there are missing pages, these will be noted. Also, if unauthorized copyright material had to be removed, a note will indicate the deletion.

UMI®

CERTIFICATE OF APPROVAL OF DISSERTATION

P-VERSION REFINEMENT STUDIES IN THE BOUNDARY ELEMENT METHOD

by

Sivakkumar Arjunon

Graduate Advisory Committee:

_____   _____
Joseph D. Richardson, Cochairperson   Date

_____   _____
Dr.Darrell E.P. Hoy, Cochairperson   Date

_____   _____
Dr.Christopher D. Wilson   Date

_____   _____
Dr.Yung-Way Liu   Date

_____   _____
Dr.John Peddieson   Date

_____   _____
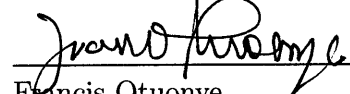Dr.George R. Buchanan   Date

_____   _____
Dr.S.Deivanayagam   Date

Approved for the Faculty:

_____
Francis Otuonye
Associate Vice President for
Research and Graduate Studies

_____
Date

ii

DEDICATION

To Divya

ACKNOWLEDGMENTS

TABLE OF CONTENTS

Page

LIST OF TABLES

LIST OF FIGURES

CHAPTER 1

INTRODUCTION

The boundary element method (BEM) has established itself as an effective numerical method for solving engineering problems in potential theory, elasticity, and acoustics. Some of the remarkable advantages of this method include reduction in the dimensionality of the problem by at least one, efficient modeling of infinite domains and accurate modeling of problems involving complex geometries and singularities.

The BEM has been implemented primarily using low order interpolations in the past, with due consideration given to the treatment of singular integrals, as analytic integration formulae for higher order elements become unavailable in closed form. Unlike the Finite Element Method, which results in a sparse system matrix, the BEM leads to dense system matrices so that using large numbers of elements as in h-version refinement is inefficient. The primary focus of this research is to advance the state of the art for higher order elements (p-version refinement) in the BEM. The use of regularized algorithms allows numerical integration which in turn can facilitate p-version refinement in the BEM. The p-version refinement can reduce the system size for a given level of accuracy, reducing computational expense. It has been observed for two-dimensional potential problems that, for a given system size, errors may be reduced by five orders of magnitude [1]. It is also mentioned solely for

reference that the dense nature of BEM systems has also spurred interest in various fast summation methods (FSM) [20, 27, 31, 30, 11]. The regularization methods in the current research target a simpler and more direct approach for computational efficiency. This document presents an overview of regularized algorithms for a collocation BEM as well as an overview of the method of fundamental solutions (MFS), followed by numerical results for p-version collocation BEM.

Among the various regularization approaches [35], whole body regularization is arguably the simplest for p-version BEM implementation [5, 19]. It has been observed that regularization and p-version refinement share some mutual dependence for their respective success [29]. The presented p-version algorithm differs significantly from other p-version algorithms [15, 14, 33, 34, 26] in terms of its ease of implementation for general problems with curved boundaries.

Many boundary element applications involve solutions of the standard boundary integral equations (SBIEs). However, problems involving coincident surfaces such as cracks and thin bodies in acoustic scattering problems show a degeneracy [9, 10]. For such problems it becomes necessary to solve the gradient boundary integral equations (GBIEs) and thus computational treatment of GBIEs involving hypersingular integrals holds significance. A weakly singular gradient boundary integral equation (BIE) formulation is therefore presented followed by a discussion of implementation strategies.

CHAPTER 2

FORMULATION AND APPROACH

The BEM can show significant computational savings over the FEM because of the inherent advantage in modeling only the boundary variables. The BEM is based on the formulation of a differential equation as a singular integral equation comprising the unknown *boundary* data. Laplace's equation,

$$\nabla^2\phi = \frac{\partial^2\phi}{\partial x^2} + \frac{\partial^2\phi}{\partial y^2} + \frac{\partial^2\phi}{\partial z^2} = 0 \tag{2.1}$$

in three dimensions for a scalar potential ϕ may be transformed into an integral form as briefly reviewed below.

2.1 Gradient BIE Formulation

Applying the divergence theorem to any two twice continuously differentiable functions ϕ and ψ, over a domain Ω with a surface Γ, and integrating by parts gives Green's second identity,

$$\int_\Omega (\phi\nabla^2\psi - \psi\nabla^2\phi)\mathrm{d}\Omega = \int_\Gamma (\phi\frac{\partial\psi}{\partial n} - \psi\frac{\partial\phi}{\partial n})\mathrm{d}\Gamma \ . \tag{2.2}$$

The key consideration in the development of the BEM is to introduce the fundamental

solution G into the second Green's identity Eq. 2.2,

$$\int_{\Omega} (\phi \nabla^2 G - G \nabla^2 \phi) d\Omega = \int_{\Gamma} (\phi \frac{\partial G}{\partial n} - G \frac{\partial \phi}{\partial n}) d\Gamma \ . \tag{2.3}$$

The fundamental solution G, also known as the free-space Green's function,

to the Laplace's equation satisfies

$$\nabla^2 G = -\mathcal{D}(\mathbf{p}, \mathbf{q}), \tag{2.4}$$

where $\mathcal{D}(\mathbf{p}, \mathbf{q})$ is the Dirac delta function, $\mathbf{p}$ and $\mathbf{q}$ are referred to as the source and

field points, respectively. The important property of the Dirac delta function is that

its value is zero everywhere except at $\mathbf{q} = \mathbf{p}$ so that the fundamental solution satisfies

Laplace's equation in the region exterior to $\mathbf{p}$. The fundamental solution of Laplace's

equation in three dimensions is [16]

$$G(\mathbf{p}, \mathbf{q}) = \frac{1}{4\pi} \left[\frac{1}{r(\mathbf{p}, \mathbf{q})} \right], \tag{2.5}$$

where $r(\mathbf{p}, \mathbf{q})$ is the distance between $\mathbf{p}$ and $\mathbf{q}$ given by

$$r(\mathbf{p}, \mathbf{q}) = \sqrt{(x_{\mathbf{p}} - x_{\mathbf{q}})^2 + (y_{\mathbf{p}} - y_{\mathbf{q}})^2 + (z_{\mathbf{p}} - z_{\mathbf{q}})^2} \ . \tag{2.6}$$

Due to the singular nature of the fundamental solution, special consideration

has to be given to the integrals in the region of $\mathbf{p}$. One approach is to surround $\mathbf{p}$ by
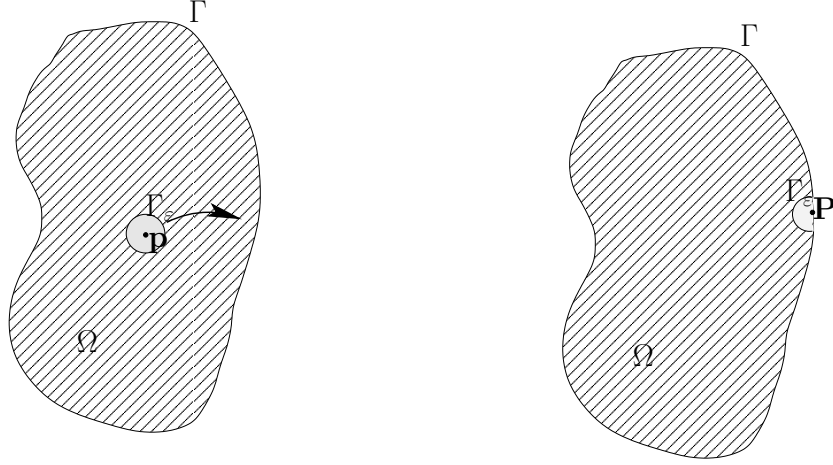
Figure 2.1: Domain with the boundary Γ and a sphere surrounding the source point P: interior and boundary forms.

a small sphere of radius ε and then to evaluate the expression in the limit as $\varepsilon \to 0$.

The region exterior to $\mathbf{p}$ is denoted as $\Omega - \Omega_\varepsilon$. In the domain $\Omega - \Omega_\varepsilon$, Eq. 2.3 becomes

$$\int_{\Omega-\Omega_\varepsilon} (\phi \nabla^2 G - G \nabla^2 \phi) \mathrm{d}A = \int_{\Gamma+\Gamma_\varepsilon} (\phi \frac{\partial G}{\partial n} - G \frac{\partial \phi}{\partial n}) \mathrm{d}\Gamma . \qquad (2.7)$$

Since ϕ and G satisfy the Laplace equation in the region exterior to $\mathbf{p}$, $\nabla^2 \phi = \nabla^2 G = 0$, and Eq. 2.7 becomes

$$0 = \int_{\Gamma} (\phi \frac{\partial G}{\partial n} - G \frac{\partial \phi}{\partial n}) \mathrm{d}\Gamma + \int_{\Gamma_\varepsilon} (\phi \frac{\partial G}{\partial n} - G \frac{\partial \phi}{\partial n}) \mathrm{d}\Gamma . \qquad (2.8)$$

The first term in the integral over Γ_ε in Eq. 2.8, written for the specific case of a sphere of radius ε, is regularized as follows:

$$\int_{\Gamma_\varepsilon} \phi(\mathbf{Q}) \frac{\partial G}{\partial n} \mathrm{d}\Gamma = \int_{\Gamma_\varepsilon} [\phi(\mathbf{Q}) - \phi(\mathbf{p})] \frac{\partial G}{\partial n} \mathrm{d}\Gamma + \phi(\mathbf{p}) \int_{\Gamma_\varepsilon} \frac{\partial G}{\partial n} \mathrm{d}\Gamma. \qquad (2.9)$$

Substituting $d\Gamma = \varepsilon^2 d\omega$, where $d\omega$ is the differential solid angle, in Eq. 2.9 gives

$$\int\limits_{\Gamma_\varepsilon} \phi(\mathbf{Q})\frac{\partial G}{\partial n}d\Gamma = \int\limits_{\Gamma_\varepsilon} [\phi(\mathbf{Q}) - \phi(\mathbf{p})]\frac{\partial G}{\partial n}\varepsilon^2 d\omega + \phi(\mathbf{p})\int\limits_{\Gamma_\varepsilon} \frac{1}{4\pi\varepsilon^2}\varepsilon^2 d\omega. \qquad (2.10)$$

When $[\phi(\mathbf{Q}) - \phi(\mathbf{p})]$ is Hölder continuous such that

$$|\phi(\mathbf{Q}) - \phi(\mathbf{p})| \leq A|r_{(\mathbf{p}\to\mathbf{Q})}|^\alpha \qquad (2.11)$$

where A and α are positive constants, the first integral on the right of Eq. 2.10

becomes 0 as $\varepsilon \to 0$,

$$\int\limits_{\Gamma_\varepsilon} \phi(\mathbf{Q})\frac{\partial G}{\partial n}d\Gamma = 0 + \phi(\mathbf{p})(\frac{4\pi}{4\pi}) = \phi(\mathbf{p}). \qquad (2.12)$$

The second term in the integral over Γ_ε in Eq. 2.8 becomes zero in the limit as $\varepsilon \to 0$

as shown below:

$$\lim_{\varepsilon\to 0}\left\{-\int\limits_{\Gamma_\varepsilon} G\frac{\partial\phi}{\partial n}d\Gamma\right\} = \lim_{\varepsilon\to 0}\left\{-\int\limits_0^{4\pi} \frac{1}{4\pi\varepsilon}\frac{\partial\phi}{\partial n}\varepsilon^2 d\omega\right\} = 0 . \qquad (2.13)$$

Thus, the third Green's identity written for interior points $\mathbf{p}$ is given as

$$\phi(\mathbf{p}) = -\int\limits_\Gamma \phi(\mathbf{Q})\frac{dG(\mathbf{p},\mathbf{Q})}{dn(\mathbf{Q})}d\Gamma(\mathbf{Q}) + \int\limits_\Gamma \frac{d\phi(\mathbf{Q})}{dn(\mathbf{Q})}Gd\Gamma(\mathbf{Q}) . \qquad (2.14)$$

It should be noted that the kernel in the first integral on the right-hand side of

Eq. 2.14,

$$\frac{dG}{dn} = \frac{-1}{r^2}(\frac{dr}{dn}) \qquad (2.15)$$

is $\mathcal{O}(\frac{1}{r^2})$ and is the differential negative of the solid angle subtended by the surface

at $\mathbf{Q}$ as seen from $\mathbf{p}$.

A square system of equations is typically generated in the BEM through a series of boundary integral equations where $\mathbf{p} \to \mathbf{P}$ on the boundary. The boundary integral equation contains a singularity and thus requires special consideration. One of several approaches is to intersect the boundary with the spherical exclusion region as shown on the right of Fig. 2.1 and then to take the limit as $\varepsilon \to 0$. The standard boundary integral equation is

$$c\phi(\mathbf{P}) + \fint_{\Gamma} \phi(\mathbf{Q}) \frac{\mathrm{d}G(\mathbf{P},\mathbf{Q})}{\mathrm{d}n} \mathrm{d}\Gamma(\mathbf{Q}) = \int_{\Gamma} \frac{\mathrm{d}\phi(\mathbf{Q})}{\mathrm{d}n} G \mathrm{d}\Gamma(\mathbf{Q}) \ . \tag{2.16}$$

In Eq. 2.16, the value of c depends on the geometry and takes the value $1/2$ for smooth surface points. The single tick mark in the integral in Eq. 2.16 implies that the integral is to be interpreted as a Cauchy Principal Value (CPV), as explained at the end of this section.

The integral representation for the flux of potential is given by the gradient of the third Green's identity. Differentiating Eq. 2.14 with respect to the source point coordinates $\mathbf{p}$ gives

$$\frac{\mathrm{d}\phi(\mathbf{p})}{\mathrm{d}x_i(\mathbf{p})} = \int_{\Gamma} \phi(\mathbf{Q}) \frac{\mathrm{d}^2 G(\mathbf{p},\mathbf{Q})}{\mathrm{d}x_i(\mathbf{Q})\mathrm{d}n(\mathbf{Q})} \mathrm{d}\Gamma(\mathbf{Q}) - \int_{\Gamma} \frac{\mathrm{d}\phi(\mathbf{Q})}{\mathrm{d}n(\mathbf{Q})} \frac{\mathrm{d}G(\mathbf{p},\mathbf{Q})}{\mathrm{d}x_i(\mathbf{Q})} \mathrm{d}\Gamma(\mathbf{Q}) \ , \tag{2.17}$$

where

$$\frac{\mathrm{d}G(\mathbf{p},\mathbf{Q})}{\mathrm{d}x(\mathbf{p})} = -\frac{\mathrm{d}G(\mathbf{p},\mathbf{Q})}{\mathrm{d}x(\mathbf{Q})} \ . \tag{2.18}$$
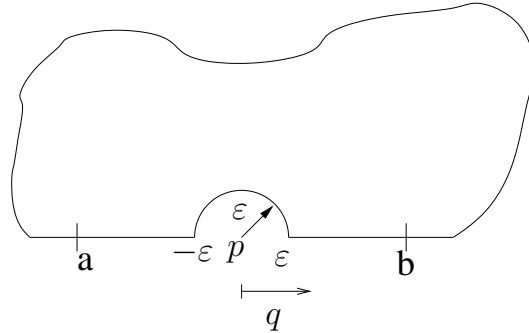
Figure 2.2: One-dimensional CPV integral.

Taking the limit to the boundary and then the inner product of the result with the normal gives the gradient BIE,

$$\frac{\mathrm{d}\phi(\mathbf{P})}{\mathrm{d}n(\mathbf{P})} = \oint_{\Gamma} \phi(\mathbf{Q})\frac{\mathrm{d}^2 G(\mathbf{P},\mathbf{Q})}{\mathrm{d}n(\mathbf{P})\mathrm{d}n(\mathbf{Q})}\mathrm{d}\Gamma(\mathbf{Q}) - \int_{\Gamma}\frac{\mathrm{d}\phi(\mathbf{Q})}{\mathrm{d}n(\mathbf{Q})}\frac{\mathrm{d}G(\mathbf{P},\mathbf{Q})}{\mathrm{d}n(\mathbf{P})}\mathrm{d}\Gamma(\mathbf{Q}) \ . \qquad (2.19)$$

The double tick mark in Eq. 2.19 implies that the integral is to be interpreted as a Hadamard finite part (HFP) [13]. A discussion of the HFP is also included at the end of this chapter.

2.1.1 Special Interpretation of Integrals

A discussion of the special interpretations of integrals is given here. The CPV of a one-dimensional integral arising from a two-dimensional problem for a function ϕ is computed by splitting it into two integrals, one on either side of the exclusion

region as shown in Fig. 2.2 as

$$\fint_a^b \frac{\phi(q)}{q-\mathbf{p}}\mathrm{d}q = \lim_{\varepsilon\to 0}\left\{\int_a^{\mathbf{p}-\varepsilon}\frac{\phi(q)}{q-\mathbf{p}}\mathrm{d}q + \int_{\mathbf{p}+\varepsilon}^b \frac{\phi(q)}{q-\mathbf{p}}\mathrm{d}q\right\}. \tag{2.20}$$

It is noted that the singular kernel in two-dimensional potential theory is $\mathcal{O}(\frac{1}{r})$ and

the hypersingular kernel is $\mathcal{O}(\frac{1}{r^2})$. Integrating the right side of Eq. 2.20 by parts gives

$$
\begin{aligned}
\fint_a^b \frac{\phi(q)}{q-\mathbf{p}}\mathrm{d}q &= \lim_{\varepsilon\to 0}\left\{\phi(q)\ln|q-\mathbf{p}|\Big|_a^{\mathbf{p}-\varepsilon} - \int_a^{\mathbf{p}-\varepsilon}\ln|q-\mathbf{p}|\frac{\mathrm{d}\phi}{\mathrm{d}q}\mathrm{d}q\right.\\
&\quad \left. + \phi(q)\ln|(q-\mathbf{p})|\Big|_{\mathbf{p}+\varepsilon}^b - \int_{\mathbf{p}+\varepsilon}^b\ln|q-\mathbf{p}|\frac{\mathrm{d}\phi}{\mathrm{d}q}\mathrm{d}q\right\}\\
&= \lim_{\varepsilon\to 0}\left\{\ln|\varepsilon|[\phi(\mathbf{p}-\varepsilon)-\phi(\mathbf{p}+\varepsilon)] - \phi(a)\ln|a-p|\right.\\
&\quad \left. +\phi(b)\ln|b-p| - \int_a^{\mathbf{p}-\varepsilon}\ln|q-\mathbf{p}|\frac{\mathrm{d}\phi}{\mathrm{d}q}\mathrm{d}q - \int_{\mathbf{p}+\varepsilon}^b\ln|q-\mathbf{p}|\frac{\mathrm{d}\phi}{\mathrm{d}q}\mathrm{d}q\right\}.
\end{aligned}
$$
$$\tag{2.21}$$

The result is finite in the limit when the coefficient of $\ln|\varepsilon|$ in Eq. 2.21 is zero which

is the case when $\phi(q) \in C^{0,\alpha}$. The contour integral over the arc of radius ε shown

in Fig. 2.2 gives rise to the free term coefficient in boundary integral formulations.

As noted earlier, the CPV shown in Eq. 2.20 exists only if $\phi(q)$ satisfies the Hölder

continuity condition given in Eq. 2.11.

The HFP is formed by differentiating the CPV given in Eq. 2.20 in accordance with Leibniz' rule [25] as

$$\frac{\mathrm{d}}{\mathrm{d}\mathbf{p}}\left\{ \fint_a^b \frac{\phi(q)}{q-\mathbf{p}}\mathrm{d}q = \lim_{\varepsilon\to 0}\left\{ \int_a^{\mathbf{p}-\varepsilon} \frac{\phi(q)}{q-\mathbf{p}}\mathrm{d}q + \int_{\mathbf{p}+\varepsilon}^b \frac{\phi(q)}{q-\mathbf{p}}\mathrm{d}q \right\} \right\} \qquad (2.22)$$

$$\begin{aligned}
\frac{\mathrm{d}}{\mathrm{d}\mathbf{p}}\left\{ \fint_a^b \frac{\phi(q)}{q-\mathbf{p}}\mathrm{d}q \right\} &= \lim_{\varepsilon\to 0}\left\{ \int_a^{\mathbf{p}-\varepsilon} \frac{\phi(q)}{(q-\mathbf{p})^2}\mathrm{d}q - \frac{\phi(\mathbf{p}-\varepsilon)}{\mathbf{p}-\varepsilon-\mathbf{p}} \right. \\
&\quad \left. + \int_{\mathbf{p}+\varepsilon}^b \frac{\phi(q)}{(q-\mathbf{p})^2}\mathrm{d}q - \frac{\phi(\mathbf{p}+\varepsilon)}{\mathbf{p}+\varepsilon-\mathbf{p}} \right\}
\end{aligned}$$

Without loss of generality, $\mathbf{p}$ can be assumed to be zero, and hence the HFP of a one-dimensional integral is given as [25]

$$\fint_a^b \frac{\phi(q)}{q^2}\mathrm{d}q = \lim_{\varepsilon\to 0}\left\{ \int_a^{-\varepsilon} \frac{\phi(q)}{q^2}\mathrm{d}q + \int_\varepsilon^b \frac{\phi(q)}{q^2}\mathrm{d}q - \frac{2\phi(0)}{\varepsilon} \right\} . \qquad (2.23)$$

The integrals on the right of Eq. 2.23, can be integrated by parts twice to give

$$\begin{aligned}
\fint_a^b \frac{\phi(q)}{q^2}\mathrm{d}q &= \left[\frac{-\phi(-\varepsilon)}{-\varepsilon} + \frac{\phi(a)}{a} \right] \\
&\quad + \left\{ [\phi'(-\varepsilon)\ln|\varepsilon| - \phi'(a)\ln|a|] - \int_a^{-\varepsilon} \ln|q|\phi''(q)\mathrm{d}q \right\} \\
&\quad + \left[-\frac{\phi(b)}{b} + \frac{\phi(\varepsilon)}{\varepsilon} \right] \\
&\quad + \left\{ [\phi'(b)\ln|b| - \phi'(\varepsilon)\ln|\varepsilon|] - \int_\varepsilon^b \ln|q|\phi''(q)\mathrm{d}q \right\} - \frac{2\phi(0)}{\varepsilon}.
\end{aligned}$$

$$(2.24)$$

The terms in Eq. 2.24 can be rearranged as

$$
\begin{aligned}
\fint_a^b \frac{\phi(q)}{q^2}\mathrm{d}q \;=\; & \underbrace{\left\{\frac{\phi(-\varepsilon)}{\varepsilon} + \frac{\phi(\varepsilon)}{\varepsilon} - \frac{2\phi(0)}{\varepsilon}\right\}}_{=0 \ for \ \phi\in C^{0,\alpha}} + \underbrace{\ln|\varepsilon|\,[\phi'(-\varepsilon) - \phi'(\varepsilon)]}_{=0 \ for \ \phi\in C^{1,\alpha}} \\
& - \ln|a|\phi'(a) + \ln|b|\phi'(b) + \frac{\phi(a)}{a} - \frac{\phi(b)}{b} \\
& - \int_a^{-\varepsilon}\ln(q)\phi''(q)\mathrm{d}q - \int_\varepsilon^b \ln(q)\phi''(q)\mathrm{d}q.
\end{aligned}
\tag{2.25}
$$

As seen in the first line of Eq. 2.25, the HFP is bounded when the density $\phi(q)$ is $C^{1,\alpha}$.

There has been some concern among BEM researchers regarding the smoothness requirements of density functions in the hypersingular integrals, many of which stem from concerns over spurious results. The validity of using C^0 elements (piecewise C^1 elements) has been questioned, based on the argument that the underlying density function in hypersingular integrals should be at least $C^{1,\alpha}$ continuous [12] for the hypersingular integrals to exist. However, the likely source of spurious results is discussed in [5, 23, 28] along with the notion of relaxed regularization which has gained some acceptance. It has been established through some successful convergence studies [29, 28, 4] that conforming C^0 boundary elements will produce very accurate numerical results when properly employed. It is noted that regularization, or any collocation method, for that matter, will fail at points where the boundary flux is singular. The proposed relaxation strategy may not be used for problems with sin-

gular surface gradients, though the need to attempt to model a singular surface flux is rare.

The following section discusses the use of regularization in order to facilitate the computational treatment of boundary integral equations .

2.2 Regularization

Regularization, in general, involves singularity reduction through the subtraction of some series expansion. The standard BIE can be regularized by subtracting $\phi(\mathbf{P})$ from the integrand with the strongly singular kernel. The gradient integral equation can be regularized by subtracting the first two terms of a Taylor series expansion of the density ϕ taken around $\mathbf{P}$ from the integrand of the integral with the hypersingular kernel. The terms added back may be computed either indirectly through comparison with simple solutions [32, 21] or through some computational approach, often based on Stokes' theorem [6]. Regularization for the gradient equation can be based on a linear state solution for the unknown field. The linear state is given by

$$\phi^{\mathsf{L}}(\mathbf{p},\mathbf{Q}) = \phi(\mathbf{p}) + \phi_{,i}(\mathbf{p})[x_i(\mathbf{Q}) - x_i(\mathbf{p})] . \tag{2.26}$$

The following relations

$$\phi(\mathbf{P}) \int_{\Gamma} \frac{\mathrm{d}^2 G(\mathbf{P},\mathbf{Q})}{\mathrm{d}n(\mathbf{P})\mathrm{d}n(\mathbf{Q})} \mathrm{d}\Gamma(\mathbf{Q}) = 0, \tag{2.27}$$
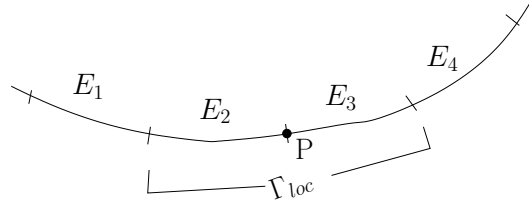
Figure 2.3: Discretized Boundary showing the local part of the boundary with source point P at the junction of second and third element.

$$\frac{d\phi(\mathbf{P})}{dn(\mathbf{P})} = \fint_{\Gamma} \phi^{\mathsf{L}}(\mathbf{P},\mathbf{Q})\frac{d^2 G(\mathbf{P},\mathbf{Q})}{dn(\mathbf{P})dn(\mathbf{Q})}d\Gamma(\mathbf{Q}) - \int_{\Gamma}\frac{d\phi^{\mathsf{L}}(\mathbf{Q})}{dn(\mathbf{Q})}\frac{dG(\mathbf{P},\mathbf{Q})}{dn(\mathbf{P})}d\Gamma(\mathbf{Q}) \qquad (2.28)$$

hold true for a closed domain, considering that a constant potential and linear variation in potential are solutions to Laplace's equation. Subtracting Eq. 2.28 from Eq. 2.19 gives the regularized form as

$$
\begin{aligned}
0 &= -\int_{\Gamma}\left[\phi(\mathbf{Q}) - \phi^{\mathsf{L}}(\mathbf{P},\mathbf{Q})\right]\frac{d^2 G(\mathbf{P},\mathbf{Q})}{dn(\mathbf{P})dn(\mathbf{Q})}d\Gamma(\mathbf{Q}) \\
&+ \int_{\Gamma}\left[\frac{d\phi(\mathbf{Q})}{dn(\mathbf{Q})} - \frac{d\phi^{\mathsf{L}}(\mathbf{Q})}{dn(\mathbf{Q})}\right]\frac{dG(\mathbf{P},\mathbf{Q})}{dn(\mathbf{P})}d\Gamma(\mathbf{Q}) .
\end{aligned}
\qquad (2.29)
$$

In Eq. 2.29 the term $[\phi(\mathbf{Q}) - \phi^{\mathsf{L}}(\mathbf{P},\mathbf{Q})]$ is $\mathcal{O}(r^2)$ and the term $[\frac{d\phi(\mathbf{Q})}{dn(\mathbf{Q})} - \frac{d\phi^{\mathsf{L}}(\mathbf{Q})}{dn(\mathbf{Q})}]$ is $\mathcal{O}(r)$ for continuous flux so that the integrals are, at most, weakly singular.

The BIEs can also be regularized by a localized approach using tangent plane regularization as shown below. The gradient BIE shown in indicial notation is

$$
\begin{aligned}
\mathcal{F}\phi_{,i}(\mathbf{p})n_i(\mathbf{P}) &= n_i(\mathbf{P})\int_{\Gamma}\phi(\mathbf{Q})G_{,ji}\,n_j(\mathbf{Q})d(\mathbf{Q})d\Gamma(\mathbf{P}) \\
&- n_i(\mathbf{P})\int_{\Gamma}\frac{d\phi}{dn}(\mathbf{Q})G_{,i}\,d\Gamma(\mathbf{Q})d\Gamma(\mathbf{P}),
\end{aligned}
\qquad (2.30)
$$

where $\mathcal{F} = 0$ for exterior problems, $\mathcal{F} = 1$ for interior problems, and $\mathcal{F} = 1/2$ for $(\mathbf{p} = \mathbf{P})$ on smooth boundaries. Considering the boundary as $\Gamma = \Gamma_{loc} + \Gamma_{non-loc}$, Eq. 2.30 can be written as

$$
\begin{aligned}
\mathcal{F}\phi_{,i}(\mathbf{P})n_i(\mathbf{P}) \;=\; & n_i(\mathbf{P}) \int_{\Gamma_{non-loc}} \phi(\mathbf{Q})G_{,ji}\,n_j(\mathbf{Q})\mathrm{d}(\mathbf{Q})\mathrm{d}\Gamma(\mathbf{P}) \\
& +n_i(\mathbf{P}) \int_{\Gamma_{loc}} \phi(\mathbf{Q})G_{,ji}\,n_j(\mathbf{Q})\mathrm{d}(\mathbf{Q})\mathrm{d}\Gamma(\mathbf{P}) \\
& -n_i(\mathbf{P}) \int_{\Gamma_{non-loc}} \frac{\mathrm{d}\phi}{\mathrm{d}n}(\mathbf{Q})G_{,i}\,\mathrm{d}\Gamma(\mathbf{Q})\mathrm{d}\Gamma(\mathbf{P}) \\
& -n_i(\mathbf{P}) \int_{\Gamma_{loc}} \frac{\mathrm{d}\phi}{\mathrm{d}n}(\mathbf{Q})G_{,i}\,\mathrm{d}\Gamma(\mathbf{Q})\mathrm{d}\Gamma(\mathbf{P}).
\end{aligned}
\tag{2.31}
$$

Regularizing the integrals over Γ_{loc} in Eq. 2.31,

$$
\begin{aligned}
\mathcal{F}\phi_{,i}(\mathbf{P})n_i(\mathbf{P}) \;=\; & n_i(\mathbf{P}) \int_{\Gamma_{non-loc}} \phi(\mathbf{Q})G_{,ji}\,n_j(\mathbf{Q})\mathrm{d}(\mathbf{Q})\mathrm{d}\Gamma(\mathbf{P}) \\
& -n_i(\mathbf{P}) \int_{\Gamma_{non-loc}} \frac{\mathrm{d}\phi}{\mathrm{d}n}(\mathbf{Q})G_{,i}\,\mathrm{d}\Gamma(\mathbf{Q})\mathrm{d}\Gamma(\mathbf{P}) \\
& +n_i(\mathbf{P}) \underbrace{\int_{\Gamma_{loc}} \left[\phi(\mathbf{Q}) - \phi(\mathbf{P}) - \phi_{,\alpha}(\mathbf{P})\xi_\alpha\right] G_{,ji}\,n_j(\mathbf{Q})\mathrm{d}\Gamma(\mathbf{Q})\mathrm{d}\Gamma(\mathbf{P})}_{Weakly\ Singular} \\
& +\; n_i(\mathbf{P})\phi(\mathbf{P}) \underbrace{\int_{\Gamma_{loc}} G_{,ji}\,n_j(\mathbf{Q})\mathrm{d}\Gamma(\mathbf{Q})}_{A_i}
\end{aligned}
$$

$$+n_i(\mathbf{P})\phi_{,\alpha}(\mathbf{P})\underbrace{\int_{\Gamma_{loc}}\xi_\alpha G_{,ji}\,n_j(\mathbf{Q})\mathrm{d}\Gamma}_{B_{i\alpha}}$$

$$-\;n_i(\mathbf{P})\underbrace{\int_{\Gamma_{loc}}\left[\frac{\mathrm{d}\phi}{\mathrm{d}n}(\mathbf{Q})-\frac{\mathrm{d}\phi}{\mathrm{d}n}(\mathbf{P})\right]G_{,i}\,\mathrm{d}\Gamma(\mathbf{Q})}_{Weakly\ Singular}$$

$$-n_i(\mathbf{P})\frac{\mathrm{d}\phi}{\mathrm{d}n}(\mathbf{P})\underbrace{\int_{\Gamma_{loc}}G_{,i}\,\mathrm{d}\Gamma(\mathbf{Q})}_{C_i}\;. \tag{2.32}$$

The term A_i may be expanded as shown below:

$$A_i=\int_{\Gamma_{loc}}G_{,ji}\,n_j(\mathbf{Q})\mathrm{d}\Gamma(\mathbf{Q})\;=\;\underbrace{\int_{\Gamma_{loc}}\left[(G_{,j})_{,i}\,n_j(\mathbf{Q})-(G_{,j})_{,j}\,n_i(\mathbf{Q})\right]\mathrm{d}\Gamma(\mathbf{Q})}_{A1_i}$$

$$+\underbrace{\int_{\Gamma_{loc}}\nabla^2 G n_i\mathrm{d}\Gamma(\mathbf{Q})}_{=0}. \tag{2.33}$$

The integral $A1_i$ can be computed using Stoke's theorem as

$$A_i=A1_i=\epsilon_{mji}\oint G_{,j}\,\mathrm{d}x_m \tag{2.34}$$

where the contour of integration is chosen to avoid the singularity as shown in Figure 2.4.

The normals in terms of the tangent plane coordinates ξ_α,ξ_β,X_3 may be written as

$$n_i(\mathbf{Q})=n_3(\mathbf{Q})\delta_{i3}+n_\beta(\mathbf{Q})\delta_{\beta i} \tag{2.35}$$
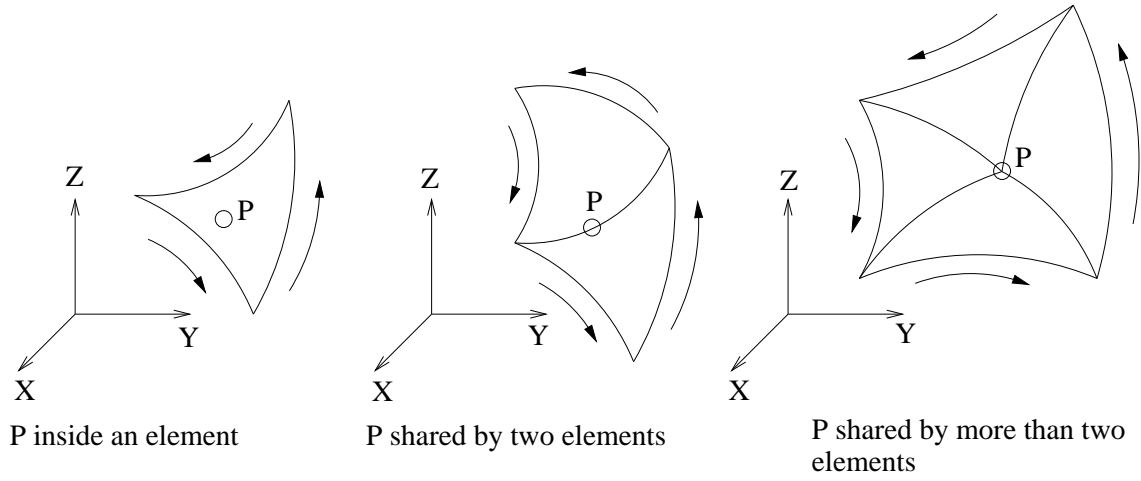
Figure 2.4: Contours for various cases of elements sharing the source point P.
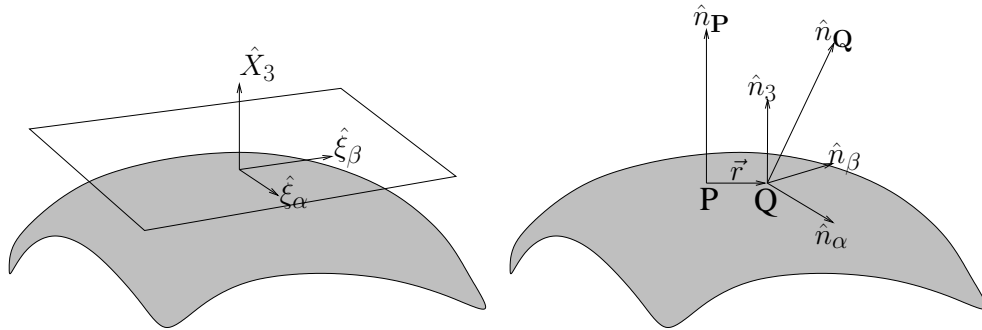
Figure 2.5: Tangent plane and normals associated with local regularization.

where the sum on β is over 1 and 2. As $\mathbf{Q}$ approaces $\mathbf{P}$, n_β tends to zero as r^2 and n_3 tends to one as shown in Figure 2.5.

The term $B_{i\alpha}$ from Eq. 2.32 may be written as follows:

$$B_{i\alpha} = \int_{\Gamma_{loc}} \xi_\alpha G_{,ji}\, n_j(\mathbf{Q})\mathrm{d}\Gamma(\mathbf{Q}) \;=\; \int_{\Gamma_{loc}} [\xi_\alpha G_{,j}]_{,i}\, n_j(\mathbf{Q})\mathrm{d}\Gamma(\mathbf{Q}) - \int_{\Gamma_{loc}} \xi_{\alpha,i} G_j n_j \mathrm{d}\Gamma(\mathbf{Q})$$

$$= \underbrace{\int_{\Gamma_{loc}} [(\xi_\alpha G_{,j})_{,i}\, n_j(\mathbf{Q}) - (\xi_\alpha G_{,j})_{,j}\, n_i(\mathbf{Q})]\, \mathrm{d}\Gamma(\mathbf{Q})}_{B1_{i\alpha}}$$

$$+ \underbrace{\int_{\Gamma_{loc}} (\xi_\alpha G_{,j})_{,j}\, n_i(\mathbf{Q})\mathrm{d}\Gamma(\mathbf{Q})}_{B2_{i\alpha}}$$

$$- \underbrace{\int_{\Gamma_{loc}} \xi_{\alpha,i} G_j n_j \mathrm{d}\Gamma(\mathbf{Q}).}_{B3_{i\alpha}}$$

$$(2.36)$$

The various terms may be treated as

$$B1_{i\alpha} \;=\; \epsilon_{mji} \oint_{\Gamma_{loc}} \xi_\alpha G_{,j}\, \mathrm{d}x_m$$

$$B2_{i\alpha} \;=\; \delta_{\alpha j} \int_{\Gamma_{loc}} G_{,j}\, n_i \mathrm{d}\Gamma + \underbrace{\int_{\Gamma_{loc}} \xi_\alpha \nabla^2 G n_i(\mathbf{Q})\mathrm{d}\Gamma}_{=0}$$

$$= \int_{\Gamma_{loc}} G_{,\alpha}\, n_i \mathrm{d}\Gamma$$

$$= \int_{\Gamma_{loc}} (G_{,\alpha}\, n_i - G_{,i}\, n_\alpha)\, \mathrm{d}\Gamma + \int_{\Gamma_{loc}} G_{,i}\, n_\alpha \mathrm{d}\Gamma$$

$$= \epsilon_{mi\alpha} \oint_{\Gamma_{loc}} G\mathrm{d}x_m + \underbrace{\int_{\Gamma_{loc}} G_{,i}\, n_\alpha \mathrm{d}\Gamma}_{B2a_{i\alpha}\,Weakly\ Singular}$$

$$B3_{i\alpha} = -\delta_{\alpha i} \int_{\Gamma_{loc}} \frac{\mathrm{d}G}{\mathrm{d}n} \mathrm{d}\Gamma.$$

$$(2.37)$$

The term C_i may be expanded as

$$C_i = \int_{\Gamma_{loc}} G_{,i} \, \mathrm{d}\Gamma(\mathbf{Q})$$

$$= \underbrace{\int_{\Gamma_{loc}} G_{,i} \left[1 - n_3(\mathbf{Q})\right] \mathrm{d}\Gamma(\mathbf{Q})}_{Weakly\ Singular} + \underbrace{\int_{\Gamma_{loc}} n_3(\mathbf{Q}) G_{,i} - n_i(\mathbf{Q}) G_{,3} \, \mathrm{d}\Gamma(\mathbf{Q})}_{C1_i}$$

$$+ \underbrace{\int_{\Gamma_{loc}} G_{,3} \, n_\alpha(\mathbf{Q}) \delta_{i\alpha} \mathrm{d}\Gamma(\mathbf{Q})}_{Weakly\ Singular} + \underbrace{\delta_{i3} \int_{\Gamma_{loc}} \frac{\mathrm{d}G}{\mathrm{d}n} \mathrm{d}\Gamma(\mathbf{Q})}_{C2_i}$$

$$- \delta_{i3} \underbrace{\int_{\Gamma_{loc}} G_{,\alpha} \, n_\alpha(\mathbf{Q}) \mathrm{d}\Gamma(\mathbf{Q})}_{Weakly\ Singular}$$

where

$$C1_i = \epsilon_{mi3} \oint_{\Gamma_{loc}} G \mathrm{d}x_m \ .$$

The Stokes' integral $\oint_{\Gamma_{loc}} G \mathrm{d}x_m$ found in $B2_{i\alpha}$ and $C1_i$ cannot be computed directly

when the source point is on the boundary of the integration region. It will be shown

that $B2_{i\alpha}$ and $C1_i$ may be combined along with their corresponding coefficients into

a single term S and evaluated over the local elements as explained below. The case

of a source node $\mathbf{P}$ on an edge is shown in Fig. 2.6. One may define $\phi^1_{,\alpha}(\mathbf{P})$ as the

gradient of ϕ associated with E_1 and $\frac{\mathrm{d}\phi^1}{\mathrm{d}n}(\mathbf{P})$ as the normal derivative associated with
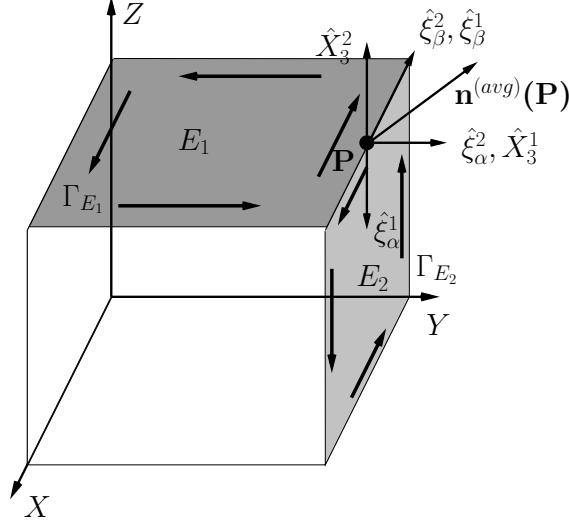
Figure 2.6: Evaluation of Stokes and Differential solid angle terms over E_1 and E_2.

E_1. For the expressions on E_1 one has

$$
\begin{aligned}
S^1 &= \epsilon_{mi\alpha} n_i^{(avg)}(\mathbf{P}) \phi_{,\alpha}^1(\mathbf{P}) \oint_{\Gamma_{E_1}} G \mathrm{d}x_m + \epsilon_{mi3} \frac{\mathrm{d}\phi^1}{\mathrm{d}n}(\mathbf{P}) n_i^{(avg)}(\mathbf{P}) \oint_{\Gamma_{E_1}} G \mathrm{d}x_m \\
&= n_i^{(avg)}(\mathbf{P}) \left[\epsilon_{mi\alpha} \phi_{,\alpha}^1(\mathbf{P}) + \epsilon_{mi3} \frac{\mathrm{d}\phi^1}{\mathrm{d}n}(\mathbf{P}) \right] \oint_{\Gamma_{E_1}} G \mathrm{d}x_m \ .
\end{aligned}
\tag{2.38}
$$

Writing $\frac{\mathrm{d}\phi^1}{\mathrm{d}n}(\mathbf{P})$ as $\phi_{,3}^1 n_3^1$ which is same as $\phi_{,3}^1$,

$$
\begin{aligned}
S^1 &= n_i^{(avg)}(\mathbf{P}) \left[\epsilon_{mi\alpha} \phi_{,\alpha}^1(\mathbf{P}) + \epsilon_{mi3} \phi_{,3}^1(\mathbf{P}) \right] \oint_{\Gamma_{E_1}} G \mathrm{d}x_m \\
&= n_i^{(avg)}(\mathbf{P}) \epsilon_{mij} \phi_{,j}^1(\mathbf{P}) \oint_{\Gamma_{E_1}} G \mathrm{d}x_m \\
&= \left[\hat{\mathbf{n}}^{(avg)}(\mathbf{P}) \times \vec{\nabla}\phi \right] \cdot \oint_{\Gamma_{E_1}} G \mathrm{d}\mathbf{x}.
\end{aligned}
\tag{2.39}
$$

Similarly, for E_2,

$$S^2 = \left[\hat{\mathbf{n}}^{(avg)}(\mathbf{P}) \times \vec{\nabla}\phi\right] \cdot \oint_{\Gamma_{E_2}} G d\mathbf{x}. \qquad (2.40)$$

It should be noted that, for the case of $\phi \in C^1$, $\vec{\nabla}\phi$ is continuous on both contours.

Therefore, the contributions on the common edge Γ_{E_1} and Γ_{E_2} will cancel due to

the reversal of the direction of the path integration on the two contours as shown in

Fig. 2.4. Though this has been shown for an edge for the present case, the results

are similarly valid for corners. Since the contributions from the common edge cancel,

the effective path of integration around the the individual areas E_1 and E_2 may be

replaced by the contour around the combined area of $E_1 + E_2$ which excludes the

common edge. Since $\mathbf{P}$ is interior to the combined area, there is no singularity on

the contour and the integral may be computed by numerical integration, combining

S^1 and S^2 according to

$$\begin{aligned} S &= S^1 + S^2 \\ &= \left[\hat{\mathbf{n}}^{(avg)}(\mathbf{P}) \times \vec{\nabla}\phi\right] \cdot \oint_{\Gamma_{(E_1+E_2)}} G d\mathbf{x}. \end{aligned} \qquad (2.41)$$

As previously mentioned, $\frac{dG}{dn}$ is $\mathcal{O}(\frac{1}{r^2})$. Various possibilities exist [22] for com-

puting the differential solid angle term $\int \frac{dG}{dn} d\Gamma$ found in $B3_{i\alpha}$ and $C2_i$. It will be

shown that the differential solid angle integrals may be combined in a manner sim-

ilar to the treatment of the contour integrals. Denoting the differential solid angle

integral on E_1 as Θ^1 and considering, for present, $\mathbf{P}$ as external to the domain, one

has Eqn. 2.42,

$$
\begin{aligned}
\Theta^1 &= \delta_{\alpha i} n_i^{(avg)}(\mathbf{P}) \phi_{,\alpha}^1(\mathbf{P}) \int_{\Gamma_{E_1}} \frac{\mathrm{d}G}{\mathrm{d}n} \mathrm{d}\Gamma + \delta_{i3} n_i^{(avg)}(\mathbf{P}) \frac{\mathrm{d}\phi^1}{\mathrm{d}n}(\mathbf{P}) \int_{\Gamma_{E_1}} \frac{\mathrm{d}G}{\mathrm{d}n} \mathrm{d}\Gamma(\mathbf{Q}) \\
&= n_\alpha^1(\mathbf{P}) \phi_{,\alpha}^1(\mathbf{P}) \int_{\Gamma_{E_1}} \frac{\mathrm{d}G}{\mathrm{d}n} \mathrm{d}\Gamma + \phi_{,3}^1(\mathbf{P}) n_3^1 \int_{\Gamma_{E_1}} \frac{\mathrm{d}G}{\mathrm{d}n} \mathrm{d}\Gamma(\mathbf{Q}) \\
&= n_\alpha^1(\mathbf{P}) \left[\phi_{,\alpha}^1(\mathbf{P}) + \phi_{,3}^1(\mathbf{P}) \right] \int_{\Gamma_{E_1}} \frac{\mathrm{d}G}{\mathrm{d}n} \mathrm{d}\Gamma(\mathbf{Q}) \\
&= \left[\hat{\mathbf{n}}_\alpha^1(\mathbf{P}) \cdot \vec{\nabla}\phi \right] \int_{\Gamma_{E_1}} \frac{\mathrm{d}G}{\mathrm{d}n} \mathrm{d}\Gamma(\mathbf{Q})
\end{aligned}
$$

where the averaged normal is written in the local coordinate system and $\frac{\mathrm{d}\phi}{\mathrm{d}n}^1$ has been written as ϕ_3^1.

Similarly, one may express the differential solid angle integral on E_2 as

$$
\Theta^2 = \left[\hat{\mathbf{n}}_\alpha^2(\mathbf{P}) \cdot \vec{\nabla}\phi \right] \int_{\Gamma_{E_2}} \frac{\mathrm{d}G}{\mathrm{d}n} \mathrm{d}\Gamma(\mathbf{Q}) \ .
$$

The motivation to combine these terms stems from the difficulty in computing each as $\mathbf{P}$ approaches an edge or corner. As before, when $\phi \in C1$ the gradient of ϕ is continuous and the integrals Θ^1 and Θ^2 have the same coefficients and therefore be combined

$$
\begin{aligned}
\Theta &= \Theta^1 + \Theta^2 \\
&= \left[\hat{\mathbf{n}}^{(avg)}(\mathbf{P}) \cdot \vec{\nabla}\phi \right] \cdot \int_{\Gamma_{(E_1+E_2)}} \frac{\mathrm{d}G}{\mathrm{d}n} \mathrm{d}\Gamma(\mathbf{Q}) \ .
\end{aligned}
\tag{2.42}
$$

The differential solid angle integrals over a boundary show a discontinuity when $\mathbf{P}$ approaches that boundary. The discontinuity is the source of the well-known jump

in the free term coefficient in BIEs. It is common in BEM formulations to embed the jump term in the free term coefficient, resulting in a complicated interpretation of differential solid angle integrals. The perspective taken in the present limit to the boundary is based on an external representation where the free term is zero. The approach taken is to let the jump term in the differential solid angle integral as $\mathbf{P}$ approaches the boundary annihilate the jump term in the free term coefficient and consider the smooth part of the differential solid angle integral. The smooth part integrates to zero over a closed surface so the integral on the local elements equals the negative of the integral on the non-local elements,

$$\Theta = -\left[\hat{\mathbf{n}}^{(avg)}(\mathbf{P}) \cdot \vec{\nabla}\phi\right] \cdot \int_{\Gamma - \Gamma_{(E_1 + E_2)}} \frac{\mathrm{d}G}{\mathrm{d}n} \mathrm{d}\Gamma(\mathbf{Q}) . \qquad (2.43)$$

It is worth noting that the fictitious enclosure method could also be employed, though this has not been employed in the present case.

In summary, the singular integrals appearing in the BIEs can be regularized; the resulting integrals added back can be decomposed into either contour integrals using Stokes' theorem or weakly singular integrals involving surface curvature or non-

singular integrals involving differential solid angles.

$$
\begin{aligned}
0 \ = \ & n_i(\mathbf{P}) \int\limits_{\Gamma_{non-loc}} \phi(\mathbf{Q})G_{,ji}\, n_j(\mathbf{Q})\mathrm{d}(\mathbf{Q})\mathrm{d}\Gamma(\mathbf{P}) \\
& -n_i(\mathbf{P}) \int\limits_{\Gamma_{non-loc}} \frac{\mathrm{d}\phi}{\mathrm{d}n}(\mathbf{Q})G_{,i}\, \mathrm{d}\Gamma(\mathbf{Q})\mathrm{d}\Gamma(\mathbf{P}) \\
& +n_i(\mathbf{P}) \underbrace{\int\limits_{\Gamma_{loc}} \left[\phi(\mathbf{Q}) - \phi(\mathbf{P}) - \phi_{,\alpha}(\mathbf{P})\xi_\alpha\right] G_{,ji}\, n_j(\mathbf{Q})\mathrm{d}\Gamma(\mathbf{Q})\mathrm{d}\Gamma(\mathbf{P})}_{Weakly\ Singular} \\
& -\ n_i(\mathbf{P}) \underbrace{\int\limits_{\Gamma_{loc}} \left[\frac{\mathrm{d}\phi}{\mathrm{d}n}(\mathbf{Q}) - \frac{\mathrm{d}\phi}{\mathrm{d}n}(\mathbf{P})\right] G_{,i}\, \mathrm{d}\Gamma(\mathbf{Q})}_{Weakly\ Singular} \\
& +\ \underbrace{n_i(\mathbf{P})\phi(\mathbf{P})\left[A1_i\right] + n_i(\mathbf{P})\phi_{,\alpha}(\mathbf{P})\left[B1_{i\alpha} + B2a_{i\alpha} + B3_{i\alpha}\right]}_{Weakly\ Singular} \\
& -\underbrace{n_i(\mathbf{P})\frac{\mathrm{d}\phi}{\mathrm{d}n}(\mathbf{P})\left[curvature\ terms\right]}_{Weakly\ Singular} \\
& +\ \left[\hat{\mathbf{n}}(\mathbf{P}) \times \vec{\nabla}\phi\right]\,.\,\oint\limits_{\Gamma_{loc}} G\mathrm{d}\mathbf{x} - \left[\hat{\mathbf{n}}(\mathbf{P})\,.\,\vec{\nabla}\phi\right]\,.\,\int\limits_{\Gamma-\Gamma_{loc}} \frac{\mathrm{d}G}{\mathrm{d}n}\mathrm{d}\Gamma(\mathbf{Q})\,.
\end{aligned}
$$

In this fashion, the integrals in the BIEs may all be computed exclusively using numerical integration.

2.3   Method of Fundamental Solutions

The method of fundamental solutions (MFS) is a class of approaches for boundary value problems for which a free-space Green's function is known. The formulation of the MFS was first proposed by Kupradze [17]. In its various implementations, the MFS avoids the singularity in the integral equations by locating the source points

outside the problem domain and building a linear system from the exterior forms of the integral identities [7]. This is equivalent to using an auxiliary boundary as done in [37]. In the current implementation, the location of external source points is investigated and a square system of linear equations is obtained by writing the external identity at different locations. It is reported that the disadvantages of the MFS may include ill-conditioned systems and reduced accuracy in comparison to the BEM [8, 38]. This reduction in accuracy may possibly be attributed to the approximations in the calculation of integrals which are nearly singular when the source points are close to the boundary. On the other hand, a possible reason for ill-conditioned systems may be due to the fact that the system of equations appears to be not linearly independent at some level of finite precision when the source points are too far from the boundary. Though the focus of the current work is the BEM, the developed algorithms can be used for MFS as well, by choosing an optimal placement of source points external to the domain.

CHAPTER 3

NUMERICAL IMPLEMENTATION

This chapter discusses the various aspects involved in numerical implementation of globally and locally regularized boundary integral formulations as discussed in Chapter 2. The numerical implementation follows the collocation procedure wherein the source point is placed at every boundary node.

In the BEM, in general, an isoparametric representation is typically taken for both the potential ϕ and its flux $\frac{\partial \phi}{\partial n}$,

$$\phi(\mathbf{Q}) \approx \phi(\xi, \eta) \; = \; \sum_{i=1}^{M} N_i(\xi, \eta) \phi^i \tag{3.1}$$

$$\frac{\partial \phi(\mathbf{Q})}{\partial n} \approx \frac{\partial \phi(\xi, \eta)}{\partial n} \; = \; \sum_{i=1}^{M} N_i(\xi, \eta) \frac{\partial \phi^i}{\partial n} \tag{3.2}$$

$$x_k(\mathbf{Q}) \approx x_k(\xi, \eta) \; = \; \sum_{i=1}^{M} N_i(\xi, \eta) x_k^i, \tag{3.3}$$

where the functions $N_j(\xi, \eta)$ are the polynomial interpolation (shape) function, ξ and η are the elemental intrinsic coordinates, and M is the number of nodes on each element. Numerical integration is performed over the boundary following the transformation to intrinsic coordinates. The integrands contain the Jacobian as part of this transformation from the physical coordinates. The Jacobian, in three dimensions, is obtained by the ratio of differential elemental area in the physical space dA
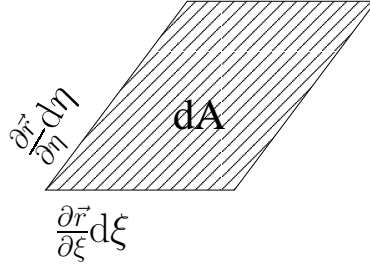
Figure 3.1: Differential area.

to the differential area of the element in the intrinsic space d$\mathcal{A}$. A differential area is given by the vector product of two differential vectors in the tangent plane as shown in Fig. 3.1. Taking

$$\vec{r}(\xi, \eta) = x(\xi, \eta)\hat{i} + y(\xi, \eta)\hat{j} + z(\xi, \eta)\hat{k} \ , \tag{3.4}$$

$$\mathrm{d}\vec{A} = \frac{\partial \vec{r}}{\partial \xi}\mathrm{d}\xi \times \frac{\partial \vec{r}}{\partial \eta}\mathrm{d}\eta = (\vec{r}_{,\xi} \times \vec{r}_{,\eta})\mathrm{d}\xi\mathrm{d}\eta \ . \tag{3.5}$$

Writing dA=J d$\mathcal{A}$, it is seen that

$$J(\xi, \eta) = |\vec{r}_{,\xi} \times \vec{r}_{,\eta}|. \tag{3.6}$$

In the linear state expression Eq. 2.26, the gradient of the unknown potential is needed in the global coordinate system. This is readily obtained through inversion of the following system.

$$\left\{ \begin{array}{c} \frac{\mathrm{d}\phi}{\mathrm{d}\xi} \\[2mm] \frac{\mathrm{d}\phi}{\mathrm{d}\eta} \\[2mm] \frac{\mathrm{d}\phi}{\mathrm{d}n} \end{array} \right\} = \left[\begin{array}{ccc} \frac{\mathrm{d}x}{\mathrm{d}\xi} & \frac{\mathrm{d}y}{\mathrm{d}\xi} & \frac{\mathrm{d}z}{\mathrm{d}\xi} \\[2mm] \frac{\mathrm{d}x}{\mathrm{d}\eta} & \frac{\mathrm{d}y}{\mathrm{d}\eta} & \frac{\mathrm{d}z}{\mathrm{d}\eta} \\[2mm] n_x & n_y & n_z \end{array} \right] \left\{ \begin{array}{c} \frac{\mathrm{d}\phi}{\mathrm{d}x} \\[2mm] \frac{\mathrm{d}\phi}{\mathrm{d}y} \\[2mm] \frac{\mathrm{d}\phi}{\mathrm{d}z} \end{array} \right\} .$$

3.1 Higher Order Elements and Shape Functions

This section explains the steps followed in the development of the shape functions associated with higher order elements as shown in [2], taking the simple case of a cubic element as an example. Triangular elements were chosen instead of quadrilateral elements based on their advantage for meshing curved surfaces. A quadratic triangular element has six nodes, three of which are corner nodes and three of which are midside nodes. A cubic element has ten nodes with one interior node at the centroid of the element. An interpolation function to represent the unknown function ϕ is given by

$$\phi = C_1 + C_2\xi + C_3\eta + C_4\xi^2 + C_5\xi\eta + C_6\eta^2 + C_7\xi^3 + C_8\xi^2\eta + C_9\xi\eta^2 + C_{10}\eta^3. \quad (3.7)$$

It should be noted that the interpolation function should be a complete polynomial represented by the Pascal's triangle as shown in Eq. 3.8. For example, the cubic

element should contain all linear, quadratic, and cubic coordinate terms.

$$1$$

$$\xi \qquad \eta$$

$$\xi^2 \qquad \xi\eta \qquad \eta^2 \longrightarrow \textit{quadratic} \uparrow (6\ \textit{terms})$$

$$\xi^3 \quad \xi^2\eta \qquad \xi\eta^2 \quad \eta^3 \longrightarrow \textit{cubic} \uparrow (10\ \textit{terms})$$

$$\xi^4 \quad \xi^3\eta \quad \xi^2\eta^2 \qquad \xi\eta^3 \quad \eta^4 \longrightarrow \textit{quartic} \uparrow (15\ \textit{terms})$$

$$\xi^5 \quad \xi^4\eta \quad \xi^3\eta^2 \qquad \xi^2\eta^3 \quad \xi\eta^4 \quad \eta^5 \longrightarrow \textit{quintic} \uparrow (21\ \textit{terms})$$

$$\xi^6 \quad \xi^5\eta \quad \xi^4\eta^2 \quad \xi^3\eta^3 \qquad \xi^2\eta^4 \quad \xi\eta^5 \quad \eta^6 \longrightarrow \textit{sextic} \uparrow (28\ \textit{terms})$$

The various constants may be written as a vector to give

$$\phi \;=\; \begin{bmatrix} 1 & \xi & \eta & \xi^2 & \xi\eta & \eta^2 & \xi^3 & \xi^2\eta & \xi\eta^2 & \eta^3 \end{bmatrix} \begin{Bmatrix} C_1 \\ C_2 \\ C_3 \\ C_4 \\ C_5 \\ C_6 \\ C_7 \\ C_8 \\ C_9 \\ C_{10} \end{Bmatrix} \tag{3.8}$$

$$=\; [\mathcal{P}^T]\{C\}.$$

Writing this for the ith node on an element and organizing a system of equations (10×10 for the cubic element) gives

$$\phi_i = C_1 + C_2\xi_i + C_3\eta_i + C_4\xi_i^2 + C_5\xi_i\eta_i + C_6\eta_i^2 + C_7\xi_i^3 + C_8\xi_i^2\eta_i + C_9\xi_i\eta_i^2 + C_{10}\eta_i^3 \,,$$

which is written in matrix form as

$$\{\phi\} = [X]\{C\} \tag{3.9}$$

where $[X]$ is a matrix involving polynomial expressions of the coordinates of nodal locations. The previous expression may be inverted to give

$$\{C\} = [X]^{-1}\{\phi\}. \tag{3.10}$$

Substituting Eq. 3.10 into Eq. 3.9, gives

$$\begin{aligned} \phi &= [\mathcal{P}^T][X]^{-1}\{\phi\} \\ &= [N]\{\phi\} \end{aligned} \tag{3.11}$$

where $[N]$ is the vector of shape functions. Computing $[\mathcal{P}^T][X]^{-1}$ using a symbolic processor, a few of the shape functions for the cubic case are given as

$$\begin{aligned} N_1 &= 1 - 5.5\xi - 5.5\eta + 9\xi^2 + 18\xi\eta + 9\eta^2 - 4.5\xi^3 \\ &\quad -13.5\xi^2\eta - 13.5\xi\eta^2 - 4.5\eta^3 \\ N_2 &= 9\xi - 22.5\xi\eta + 27\xi^2\eta + 13.5\xi\eta^2 - 22.5\xi^2 + 13.5\xi^3 \\ &\vdots \\ N_{10} &= 27\xi\eta - 27\xi^2\eta - 27\xi\eta^2. \end{aligned}$$

The general methodology can be extended for deriving shape functions of any order.
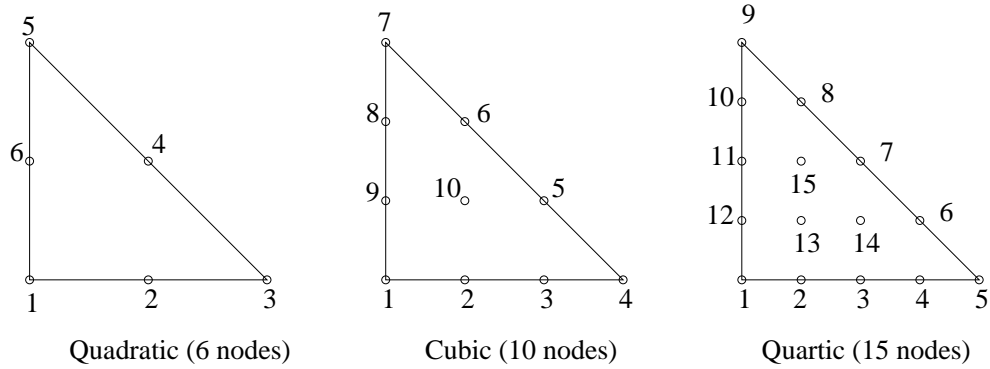
Figure 3.2: Node placement and numbering for quadratic, cubic, quartic elements.

This method for the development of shape functions leads to increasingly large systems for increasing element orders. However, the availability of symbolic computational tools makes the implementation tractable. The symbolic processor used in this work was Maple® which can output code in several programming languages including Fortran. One needs to have only the polynomial vector $[\mathcal{P}^T]$ and the nodal locations matrix $[X]$ of a particular order to derive the corresponding shape functions.

The node numbering sequence and the node placement, shown in Figure 3.2 for the quadratic, cubic, and quartic elements, can be arbitrary. However for the sake of simplicity, the node placement has been chosen to follow a pattern of similar triangles. Though it is possible to derive shape functions for an element of any order, for the current study only the elements shown in Table 3.1 have been formulated. It is also noted that numerical results are presented only for cubic, quartic, sextic, and

Table 3.1: p-version elements.

Element	No. of nodes
Quadratic	6
Cubic	10
Quartic	15
Sextic	28
Octic	45
9th order	55
12th order	91
16th order	153

octic element types. Motivation for the choice of these elements stemmed from the fact that the mesh generation technique described in the next section required prime factors of two and three due to constraints in the meshing software.

3.2   Mesh Generation

The lack of higher order elements in the element library of commercial meshers makes discretization of the model geometry using p-version elements a challenging task. In the current study, the test geometry was meshed with higher order elements using some macros written for the commercial finite element software ANSYS. The element refinement capabilities of the software was used to generate elements of various orders. The geometry was first modeled using 3-noded linear triangular elements and then successively refined to generate nodes in the same pattern as that of the standard p-version elements formulated in the previous section, and shown for a cu-

Single 3–noded element   Element refined into nine 3–noded elements   Nodes picked from the refined mesh to form one 10–noded cubic element
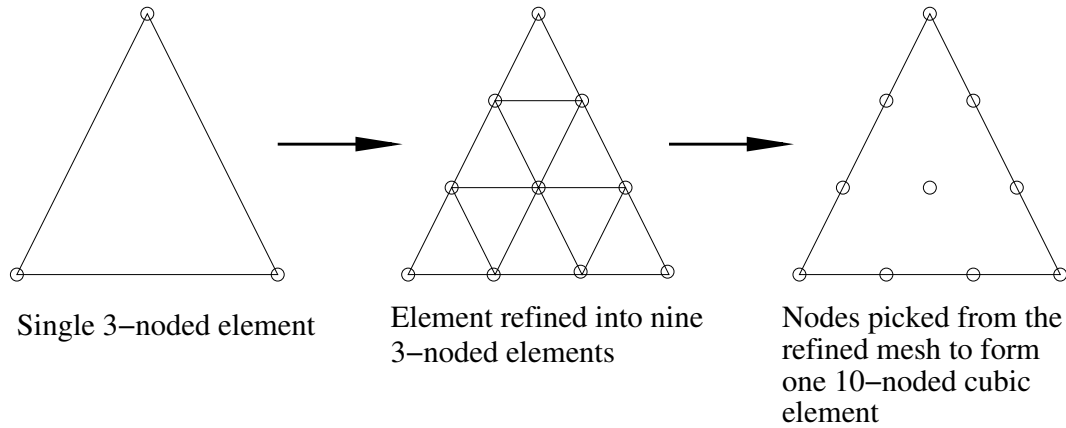
Figure 3.3: Mesh generation with cubic elements using ANSYS.

bic case in Figure 3.3. As previously mentioned, the refinement selections available in ANSYS limit the present consideration to elements of orders of prime factors of two and three. The current approach works well for flat surfaces and the area of a tetrahedron intercepting coordinate axes at one was calculated to fifteen significant figures of accuracy using cubic, quartic, sextic, octic, and 9th order elements. However, this approach generates some distortion while meshing curved boundaries. The optimal node placement on curved geometries is an ongoing task outside the scope of the present effort.

3.3   Numerical Integration Rules for Triangles

The presence of integrals which have kernels of reciprocal powers in $|r(\mathbf{p}, \mathbf{q})|$ in conjunction with systems which are not particularly well-conditioned requires ac-
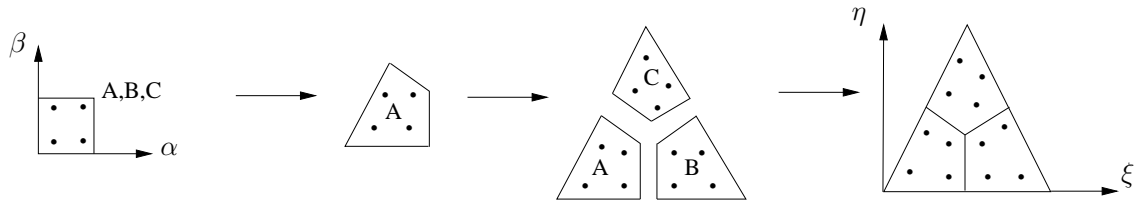
Figure 3.4: Development of a 2-D 12-point scheme from 2×2 schemes on quadrilaterals.

curate integration schemes. Since numerical integration will be used in the proposed algorithms, the effort was focused on developing much higher order Gaussian quadrature schemes than those commonly used. Cowper [3] has provided quadrature formulae for symmetrically placed points, though this approach cannot be extended to very high orders of integration since the equations for the sampling point locations and weights are nonlinear and cannot be solved easily. Lynnes and Jesperson [24] have listed rules using polar coordinates, that can integrate any polynomial of degree eleven, while Laursen and Gellert [18] have suggested symmetric integration formulae of tenth degree precision. Even though specific transformation formulae are available to integrate specific weakly singular integrals, [36, 39] for the sake of simplicity, in the current work two classes of higher order Gaussian quadrature schemes for a triangle with vertex coordinates (0,0), (0,1), (1,0) were developed. The first class of quadrature rules were developed by first considering an N×N scheme on multiple quadrilateral regions and then mapping these quadrilaterals to the triangle. The

Table 3.2: Higher order quadrature schemes.

N× N scheme	3 quads	5 quads
2× 2	12	20
⋮	⋮	⋮
10× 10	300	500
12× 12	432	720
14× 14	588	980
16× 16	768	1280
18× 18	588	1620
20× 20	1200	2000
32× 32	3072	5120
64× 64	12288	20480
96× 96	27648	46080

number of points in the quadrature scheme depends on the number of quadrilaterals mapped onto the triangle and the order of integration on each quadrilateral. The various schemes are shown in Table 3.2. For example, when the triangle is sub-divided into five quadrilaterals, each with an 8×8 rule, a 320 point $(8 \times 8 \times 5)$ rule is obtained for the triangle. This 320 point rule can be applied to evaluate an integral of any function $f(\xi, \eta)$ over the triangle as

$$\int_\Delta f(\xi,\eta)\mathrm{d}\xi\mathrm{d}\eta \approx \sum_{i=1}^{5}\sum_{j=1}^{8}\sum_{k=1}^{8} f^i(\alpha_j^i,\beta_k^i)J^i(\alpha_j^i,\beta_k^i)w_jw_k = \sum_{l=1}^{320} f(\alpha_l,\beta_l)W_l \ . \quad (3.12)$$

where $W_l = J^i(\alpha_j^i,\beta_k^i)w_jw_k$. It is noted that α and β are taken from sampling the one-dimensional Gaussian quadrature and J is the Jacobian of the transformation of the quadrilaterals from their orientation on the triangle. A list of some of the schemes generated is shown in Table 3.2.
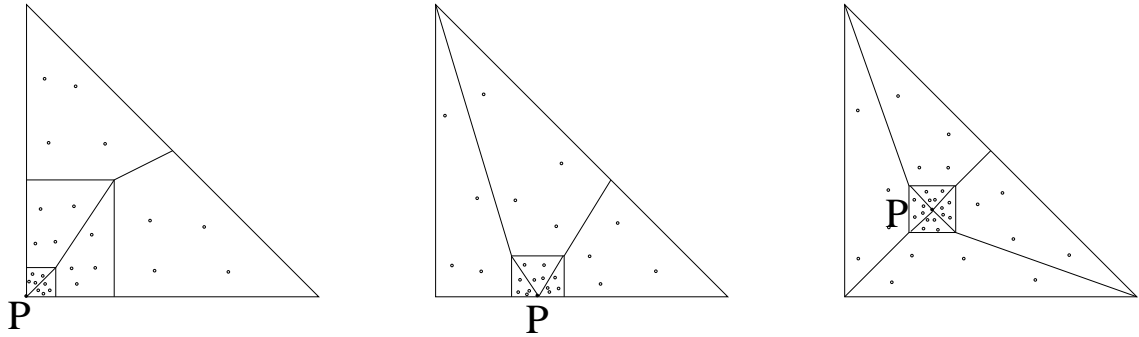
Figure 3.5: Development of a quadrature rule for cubic element for corner, side and interior source point locations

These first class of integration routines, though effective when used with the method of fundamental solutions, was not very accurate when it came to calculating the integrals with kernels involving inverse powers of $|r(\mathbf{p}, \mathbf{q})|$ in the boundary element method. This was evident when these integration rules were used to integrate $1/r(\mathbf{p}, \mathbf{q})$ over a triangular region 3.3. This necessitated the development of the second class of quadrature rules. In the second class of quadrature rules, separate schemes were developed for each element type. For example, a cubic model has an exclusive quadrature rule with a separate set of abscissas and weights for each of the ten nodes. Similarly, quartic elements have separate schemes for each of the fifteen nodes. The basic idea behind this approach is to increase the density of integration points so that the steep variation of integrands is accurately sampled. This is achieved by mapping nonuniform quadrilateral regions, each with different N×N

Table 3.3: $1/r$ calculation over a triangle using class I and class II rules for various locations of source point **P**

P location	Exact	Class I		Class II	
		12288 rule	32768 rule	Cubic rule	Octic rule
(0,0)	1.2464504802	1.27	1.26	1.246450479	1.246450481
(1,0)	0.8813735870	0.878	0.879	0.881373586	0.8813735871
(0,1)	0.8813735870	0.878	0.879	0.881373585	0.8813735869
(1/3,1/3)	2.4072299231	2.39	2.39	2.407230	2.4072294
(1/3,0)	1.7021686025	1.67	1.69	1.70216862	1.70216809

scheme, to the triangle. Smaller triangles (degenerate quadrilaterals) with a higher N×N scheme surround and taper towards the considered nodal location, whereas bigger quadrilaterals with a lower N×N scheme map to the region away from the nodal location. This is shown in Fig. 3.5. For example, a quadrature scheme for the interior node of a cubic element is developed by mapping four triangles around the interior node and four comparatively bigger quadrilaterals in the region away from the node. Fig. 3.5 shows the case for a corner node and an edge node as well. The number of points for each of these rules depends on the number of quadrilaterals mapped to the triangle and the order of integration on each quadrilateral. These second class of rules performed better than the previous class of rules when it was used to integrate $1/r(\mathbf{p}, \mathbf{q})$ over a triangle as shown in Table 3.3.

CHAPTER 4

RESULTS

The algorithms developed for the weakly singular boundary integral formulations were tested on flat and curved surface geometries. A tetrahedron, though considered for a flat surface geometry, is typically considered problematic due to its edges and corners. The approaches developed in the current work can be applied for smooth surfaces as well as surfaces with edges and corners. It is also noted that patch test problems on the tetrahedron involving linear potentials were solved accurately to around nine digits.

4.1   Example 1

The results of a heat conduction problem in a tetrahedron solved using the globally-regularized weakly singular gradient BEM formulation is presented here. The tetrahedron and the imposed boundary conditions are shown in Fig. 4.1. The tetrahedron was meshed with higher order elements using the approach explained in Chapter 3. A temperature boundary condition was applied on one node on the oblique face and flux boundary conditions were given elsewhere. The problem is based on an
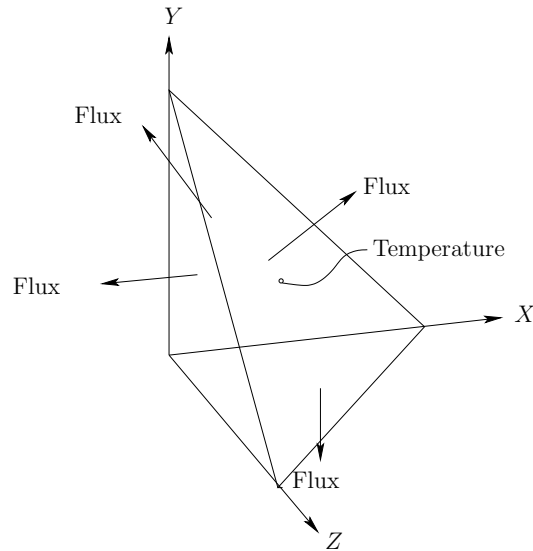
Figure 4.1: Boundary conditions on Tetrahedron.

eigensolution given by

$$\phi = e^{4.7x}sin(4.7y + 11) + e^{4.7y}sin(4.7z + 11) + e^{4.7z}sin(4.7x + 11). \qquad (4.1)$$

The factors 4.7 and 11 in Eq. 4.1 were chosen arbitrarily to pose a problem with steep gradients and without symmetry.

The nodal results for temperature, when modeled using a single element on each face of the tetrahedron, for various element orders are shown in Fig. 4.2. The nodal results for the temperature are plotted along one of the edges of the tetrahedron as shown in Fig. 4.3. As inferred from the plot, a single octic element models the temperature distribution to a high level of accuracy whereas three cubic elements show some prominent errors, especially in the corners, in spite of having around 20%
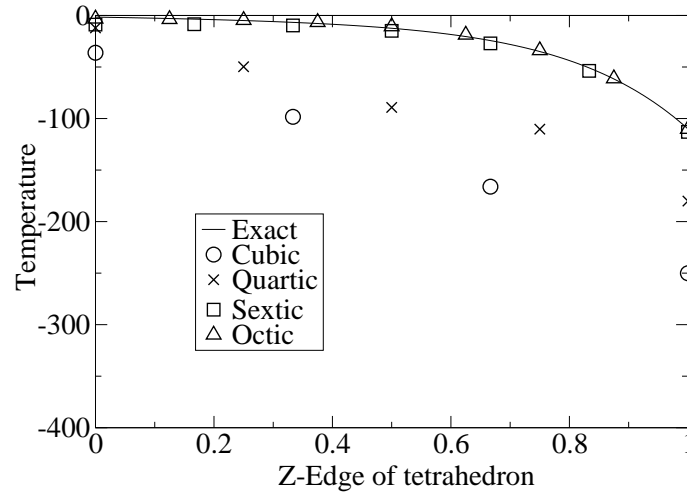
Figure 4.2: Example 1: Temperature along one of the edges using different element types

more degrees of freedom (DOF) (130 nodes in the octic model and 164 nodes in the cubic model). An average error may be defined as

$$\text{Error} = \frac{\sum\limits_{i=1}^{nodes} \frac{\phi_i^{Exact} - \phi_i^{BEM}}{|\phi_i^{Max} - \phi_i^{Min}|}}{\text{Number of nodes}} \qquad (4.2)$$

The errors for various elemental orders, shown in Table 4.1, indicate that the octic elements show errors that are three orders of magnitude less than when using cubic elements.

4.2   Example 2

As a second example, the problem defined in previous example is solved using *locally*-regularized weakly singular gradient BEM formulation. The errors associated
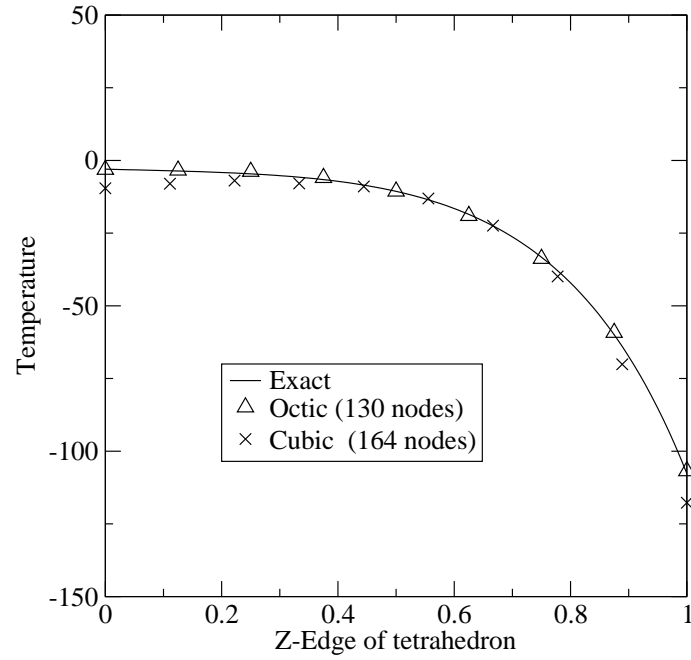
Figure 4.3: Example 1 : Temperature along one of the edges computed using a three cubic elements and single octic element using globally regularized BEM.

Table 4.1: Temperature results on tetrahedron using globally regularized BEM.

Element	Error
Cubic	1.0575
Quartic	0.5243
Sextic	0.0947
Octic	0.0083

Table 4.2: Temperature results on tetrahedron using locally regularized BEM.

Element	Error
Cubic	0.7572
Quartic	0.0437
Sextic	0.0143
Octic	0.0009

with various elemental order models of the tetrahedron are shown in Table 4.2.

The locally regularized weakly singular gradient BEM algorithm performs better than the globally regularized form for cubic and quartic element types by roughly an order or magnitude. This is attributed to better approximation of the density functions in the locally regularized form as the subtracted Taylor's series terms are added back in an indirect form which is not the case in the globally regularized form. This was suggested as a cause for difference in accuracy seen in locally and globally regularized BEM given in [4].

4.3   Example 3

A unit sphere with Dirichlet boundary conditions is solved using locally-regularized gradient BEM formulation. A temperature variation of $\phi = x^2 + y^2 - 2z^2$ is applied.

It is important to note that there are significant differences between modeling flat surfaces and curved surfaces. For the case of curved surfaces there is generally

distortion in the transformation so that the only field which can be exactly inter-polated is a uniform field regardless of element order. However, it is observed that, for curved surfaces, the representation becomes increasingly accurate with p-version refinement. Also, the mesh generation approach discussed in Chapter 3 was not en-tirely successful for geometries with curved surfaces as the two commercial meshers which were investigated introduced excessive distortion. The primary advisor of this dissertation developed a stochastic mesh optimization algorithm on spherical surfaces which was used to generate higher order elemental meshes on the spherical surface.

The sphere was modeled using eight elements with a single element stretching across each octant. The flux results show symmetry across the three coordinate axes. The results from various higher order element models are shown in Fig. 4.4 for just one octant of the sphere on the Y-Z plane. The plot 4.4 once again shows the enhancement in accuracy with p-version refinement. Table 4.3 shows the comparison of flux calculated by different element orders at location(0,0,1).
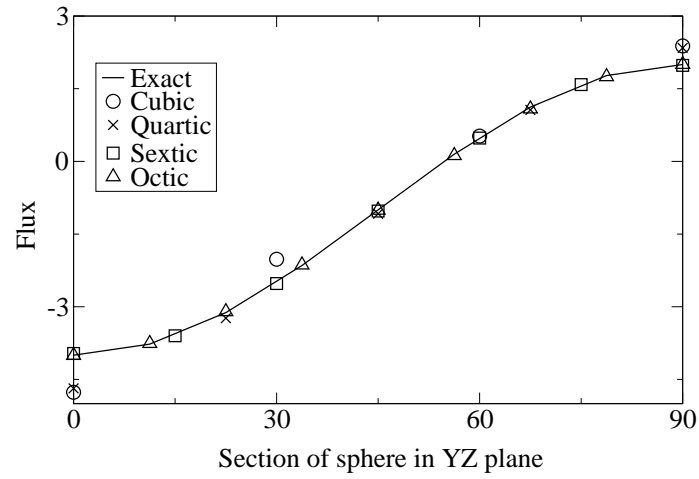
Figure 4.4: Example 3: Flux variation on sphere from $\theta = 0$ to $\theta = 90$ on Y-Z plane

Table 4.3: Example 3: Flux values at (0,0,1).

Element	Flux
	Exact flux=-4.00000
Cubic	-4.765
Quartic	-4.685
Sextic	-3.963
Octic	-4.004

CHAPTER 5

CONCLUSION

The primary focus of the research was the development of weakly singular gradient BEM formulations in 3D and its numerical implementation. The presented approaches are focused on simplicity and ease of implementation, so that any element type may be used due to the fact that the weakly singular integrals can be computed using numerical integration. The regularization has been shown in both global and local forms. The computational strategy for the locally regularized BEM follows an external limit to the boundary of the domain and effectively computes its free term as part of the regularization. The whole body regularized form has no free term. Also, it is significant to note that the formulations can be used for geometries with flat or curved surfaces with edges and corners. The primary advisor for this work developed a stochastic mesh optimization algorithm, limited only to spherical surfaces. New quadrature rules were developed, validated, and implemented.

The tetrahedron was solved for a highly varying potential with steeply varying gradients. The results show significant improvements in accuracy with every p-version refinement. An octic model showed a decrease in error by an order of magnitude using the globally regularized BEM, though the cubic model 20% more degrees of freedom. The numerical results show the advantages in using p-version elements.

Though problems involving simple geometries were considered in the current study, it is predicted that the benefits of using p-version elements will be enhanced for bigger and more complex geometries, subject to the possibility of accurate representation of curved surface geometries and boundary data for cases involving potentials with steeply varying gradients. For a given element order the local form is shown to be more accurate [4].

BIBLIOGRAPHY

[1] S. Arjunon and J. D. Richardson. Regularized p-version collocation BEM algorithms for two-dimensional heat conduction. *Engineering Analysis with Boundary Elements*, 29:953–962, 2005.

[2] George R. Buchanan. *Schaum's Outline of Theory and Problems of Finite Element Analysis*. McGraw-Hill, New York, 1994.

[3] G. R. Cowper. Gaussian quadrature formulas for triangles. *Int. J. Num. Meth. Engrg.*, 7:405–408, 1972.

[4] T. A. Cruse and J. D Richardson. Weakly singular stress-BEM for 2D elastostatics. *Int. J. Num. Meth. Engrg.*, 45:13–35, 1999.

[5] T. A. Cruse and J. D. Richardson. *Self-Regularized Hypersingular* BEM *for Laplace's Equation Mathematical Aspects of Boundary Element Methods*. Chapman and Hall/CRC, London, 2000.

[6] T. A. Cruse and W. Suwito. On the somigliana stress identity in elasticity. *Comput. Mech.*, 11:1–10, 1993.

[7] Graeme Fairweather and Andreas Karageorghis. The method of fundamental solutions for elliptic boundary value problems. *Advances in Computational Mathematics*, 9:69–95, 1998.

[8] G. S. A. Fam and Y. F. Rashed. *Boundary Elements XXIV*. Wessex Institute of Technology, Southampton,UK, 1999.

[9] A. Frangi. Fracture propogation in 3D by the symmetric galerkin boundary element method. *International Journal of Fracture*, 116:313–330, 2002.

[10] A. Frangi, G. Novati, and R. Springhetti. *Symmetric Galerkin Boundary Element Analysis in Three-dimensional Linear-elastic Fracture Mechanics Boundary Element Methods for Soil-Structure Interaction*. Kluwer Academic Publishers, Netherlands, 2003.

[11] J. E. Gomez and H. Power. A multipole direct and indirect BEM for 2D cavity flow at low reynolds number. *Engineering Analysis with Boundary Elements*, 19:17–31, 1997.

[12] M. Guiggiani, G. Krishnasamy, T. J. Rudolphi, and F. J. Rizzo. A general algorithm for the numerical solution of hypersingular boundary integral equations. *J. Appl. Mech. ASME*, 59:604–614, 1992.

[13] J. Hadamard. *Lectures on Cauchy's Problem in Linear Partial Differential Equations*. Yale University Press, 1923.

[14] S. M. Holzer. The *h-*,*p-* and *hp-* versions of the bem in elasticity: numerical results. *Commun Numer Method Eng*, 11:255–65, 1995.

[15] Stefan M. Holzer. A *p*-extension of the symmetric boundary element method. *Computer methods in applied mechanical engineering*, 115:339–357, 1993.

[16] D. Kellogg. *Foundations of Potential Theory*. Dover Publications, New York, 2007.

[17] V. D. Kupradze and M. A. Aleksidze. The method of functional equations for the approximate solution of certain boundary value problems. *Comput. Math. Math. Phys*, 4:82–126, 1964.

[18] M. E. Laursen and M. Gellert. Some criteria for numerically integrated matrices and quadrature formulas for triangles. *Int. J. Num. Meth. Engrg.*, 12:67–76, 1978.

[19] Y. J. Liu. On the simple-solution method and non-singular nature of the BIE/BEM - a review and some new results. *Engineering Analysis with Boundary Elements*, 24:789–795, 2000.

[20] Y. J. Liu, N. Nishimura, and Z. H. Yao. A fast multipole method accelerated method of fundamental solutions for potential problems. *Engineering Analysis with Boundary Elements*, 29:1016–1024, 2005.

[21] Y. J. Liu and T. J. Rudolphi. New identities for fundamental solutions and their applications to non-singular boundary element formulations. *Comput. Mech.*, 24:286–292, 1999.

[22] Yijun Liu. Analysis of shell-like structures by the boundary element method based on 3-D elasticity: formulation and verification. *Int. J. Num. Meth. Engrg.*, 41:541–558, 1998.

[23] Yijun Liu and Shahoi Chen. A new form of the hypersingular boundary integral equation for 3-d acoustics and its implementation with c^0 boundary elements. *Computer methods in applied mechanical engineering*, 173:375–386, 1998.

[24] J. N. Lynnes and D. Jespersen. Moderate degree symmetric quadrature rules for the triangle. *J. Inst. Math. Applic.*, 15:19–32, 1973.

[25] P. A. Martin and F. J. Rizzo. Hypesingular integrals: how smooth must the density be? *Int. J. Num. Meth. Engrg.*, 39:687–704, 1996.

[26] N. mellado N. Heuer and E. P. Stephan. A *p*-adaptive algorithm for the bem with the hypersingular operator on the plane screen. *Int. J. Num. Meth. Engrg.*, 53:85–104, 2002.

[27] A. P. Peirce and J. A. L. Napier. A spectral multipole method for efficient solution of large-scale boundary element models in elastostatics. *Int. J. Num. Meth. Engrg.*, 38:4009–1034, 1995.

[28] J. D. Richardson. On the validity of conforming bem algorithms for hypersingular boundary integral equations. *Comput. Mech.*, 20:213–220, 1997.

[29] J. D. Richardson. Numerical *p*-version refinement studies for the regularized stress-bem. *Int. J. Num. Meth. Engrg.*, 58:2161–2176, 2003.

[30] J. D. Richardson, L. J. Gray, T. Kaplan, and J. A. L. Napier. A regularized spectral bem for plane elasticity. *Engineering Analysis with Boundary Elements*, 25:297–311, 2001.

[31] V. Rokhlin. Rapid solution of integral equations of classical potential theory. *Journal of Computational Physics*, 60:187–207, 1985.

[32] T. J. Rudolphi. The use of simple solutions in the regularization of hypersingular boundary integral equations. *Mathl. Comput. Modelling*, 15:269–278, 1991.

[33] E. P. Stephan and F. V. Fostell. On the *h*-,*p*- and *hp*- versions of the boundary element method-numerical results. *Comput Methods Appl Mech Eng*, 83:69–89, 1990.

[34] E. P. Stephan and M. Suri. On the convergence of the *p*-version of the boundary element galerkin method. *Math Comput*, 52:31–48, 1989.

[35] M. Tanaka, V. Sladek, and J. Sladek. Regularization techniques applied to boundary element methods. *Applied Mechanics Reviews*, 47:457–499, 1994.

[36] Douglas J. Taylor. Accurate and efficient numerical integration of weakly singular integrals in galerkin efie solutions. *IEEE Transactions on Antennas and Propogation*, 51:1630–1637, 2003.

[37] W. W. Schultz Y. Cao and R. F. Beck. Three-dimensional desingularized boundary integral method for potential problems. *Int. J. Num. Meth. Engrg.*, 12:785–803, 1991.

[38] D. L. Young, S. J. Jane, CM Fan, K Murugesan, and C C Tsai. The method of fundamental solutions for 2D and 3D stokes problems. *Journal of Computational Physics*, 211:1–8, 2006.

[39] Beong In Yun and Philsu Kim. A new sigmoidal transformation for weakly singular integrals in the boundary element method. *SIAM J. Sci. Statist. Comp.*, 24:1203–1217, 2003.

VITA

Sivakkumar Arjunon was born in Chennai, Tamil Nadu, India. He graduated from High School in 1996 majoring in Math, Physics, Chemistry and Biology. He entered Government College of Engineering, Tirunelveli, India (affiliated to Manonmaniam Sundaranar University) in 1997 and received the Bachelor of Engineering in 2001. He pursued his Master's degree in Mechanical Engineering at Tennessee Technological University (TTU). He then worked towards PhD in Engineering at TTU starting in 2003. While pursuing his doctoral degree he worked as research assistant, instructor, and simulation and analysis engineer with an automotive parts supplier company.